JOURNAL OF MATERIALS SCIENCE 25 (1990) 4120–4124

Ammonia gas nitriding of Fe–18Cr–9Ni alloy at lower than 823 K

HIDEYUKI KUWAHARA, HIROAKI MATSUOKA
Research Institute for Applied Sciences, Tanaka-Oicho, Sakyo-ku, Kyoto 606, Japan
JUN TAKADA
Department of Applied Chemistry, Okayama University, Tsushima-Naka, Okayama 700, Japan
SHIOMI KIKUCHI, YOUICHI TOMII
Department of Metal Science and Technology, Kyoto University, Sakyo-ku, Kyoto 606, Japan
TORU TAKAYAMA
Advanced Technology Research Laboratories, Physical and Chemical Analysis Research Laboratory, Sumitomo Metal Industries Ltd, Nishinagasu-Hondori, Amagasaki 660, Japan

An Fe–18Cr–9Ni alloy, which it had not previously been possible to nitride at temperatures below 873 K, was found to form nitrides in an ammonia gas atmosphere at temperatures as low as 823 K after annealing at low hydrogen pressure at 1473 K. Microstructure and hardness were examined on cross-sections of the nitrided specimens. An internal nitriding layer had formed beneath an external nitriding layer on the specimen surface. Vickers hardness was above 1000 throughout the internal nitriding layer. The nitrides formed at the specimen surface and in the internal nitriding layer were identified using grazing incidence X-ray diffraction and ordinary X-ray diffraction methods, respectively. The external nitriding layer, which was about 6 to 10 μm thick, formed on the surface, which consisted of ε–$Fe_{2-3}N$, γ'–Fe_4N, and CrN. Two types of chromium nitride were precipitated by ammonia gas nitriding of the present alloy: CrN in the external nitriding layer and Cr_2N in the internal nitriding layer.

1. Introduction

Steels are usually strengthened by quenching, carburizing and quenching, or nitriding, etc. Ammonia gas nitriding of steels forms nitrided layers at and below the specimen surface. The thin external layer, which consists of one or more iron nitrides, improves both the wear and corrosion resistance of the alloy. The alloy is further strengthened by the dissolution of nitrogen and sometimes the precipitation of nitrides in the thicker internal layer. Nitriding is thus usually applied to the steels used for machine and automobile parts.

Because the martensite start temperature, M_s, is considerably lower than room temperature, it is not normally possible to strengthen austenitic iron alloys with high chromium content (for example, Fe–18Cr–9Ni) by quenching. However, nitriding can be used to strengthen these alloys because of the precipitation of chromium nitride in the nitriding layer and the formation of iron nitrides on the specimen surface. In practice, these steels are gas nitrided at temperatures greater than 873 K, although lower temperatures are desirable in order to suppress plastic deformation due to residual stress and to increase strength by the precipitation of fine nitrides.

In the ammonia gas nitriding of high chromium iron alloys at temperatures below 873 K, two problems exist: the difficulty of ammonia gas nitriding of these alloys, and the identification of chromium nitride. In order to solve these problems, most investigators use acid solutions [1, 2]. Gas nitriding of AISI 316L alloy at 773 and 823 K only resulted in the formation of a thin nitriding layer, which was uneven and not well defined. Moreover, the nitriding layer on AISI 316L alloy at temperatures lower than 823 K had poor reproducibility [3]. The difficulty of nitriding high chromium alloys at temperatures below 873 K may result from the existence of a layer of surface oxides, especially chromium oxide. Although most investigators used various acid solutions in order to remove the oxide layer [1–3], the poor reproducibility of a thin nitriding layer which was uneven and well defined may be ascribed to the retained oxide. It is, therefore, desirable to develop a process for removing the chromium oxide layer on the surface of high chromium alloys, including stainless steels. We show here that even if an acid solution is used to remove the oxide layer from high chromium specimens, the layer reforms as soon as the specimen is exposed to air. If the surface oxide layer can be prevented from reforming, ammonia gas nitriding of high chromium alloys may be achieved at temperatures below 873 K.

There have been numerous investigations into the precipitation of chromium nitride; Cr_2N precipitated in Fe–18Cr–8Ni alloy [4], CrN in the γ-phase matrix and Cr_2N with α-phase precipitated by ammonia gas

0022–2461/90 $03.00 + .12

nitriding of AISI 316L alloy in the temperature range 873 to 1073 K [3], CrN precipitated in the α-matrix by an ammonia gas nitriding of Fe–14Cr at 1168 K [2] and also by plasma nitriding of Fe–19Cr alloy at 803 K [5]. If a high chromium alloy can be nitrided using ammonia gas at the low temperature of 823 K, it should be possible to identify whether the precipitate is CrN or Cr_2N in the nitriding layer and to be then possible to make the mechanism for nitriding these alloys using ammonia gas.

The grazing incidence X-ray diffraction technique (GIXD) is used for analysing changes in structure with distance from the surface when AISI 304L and 321 alloys are modified by ion implantation of nitrogen [6]. Because it reveals the structure of extremely thin layers, GIXD can be used to distinguish the changes in phases formed at the surface.

To investigate the possibility of nitriding high chromium alloys at temperatures below 873 K which, from previous studies, is the lowest temperature for successful gas nitriding of high chromium alloys, Fe–18Cr–9Ni alloy, which is representative of austenitic stainless steels, was nitrided using an *in situ* method of hydrogen annealing to remove the oxide layer. The microstructure was observed and the hardness measured, and the nitrides examined using GIXD and conventional X-ray diffraction (2θ–θ or Bragg–Brentano).

2. Material and experimental procedure

Fe–18Cr–9Ni alloy of chemical composition shown in Table I, was cut into 10 × 15 × 5 mm^3 specimens. These specimens were mechanically polished using a buff with diamond paste, and the surface then cleaned in acetone using an ultrasonic cleaner. The specimens were first annealed in a low-pressure hydrogen atmosphere of 0.107 kPa (0.8 Torr, measured by Pirani gauge) at 1473 K for 3.6 ksec, followed by cooling to room temperature under the same atmosphere. This annealing was carried out in order to homogenize the specimens and to remove the oxide layer on the specimen surface. The specimens were heated to the nitriding temperature immediately after hydrogen annealing and cooling, without being exposed to air at any time. This was to prevent the formation of surface oxides. Ammonia gas nitriding was carried out at 823 K for 68.4 ksec at a pressure of 0.1 MPa (760 Torr). The temperature was controlled to within ±2 K during annealing and nitriding.

The nitrided specimens were carefully cut into halves parallel to one of their surfaces. Cross sections were mechanically polished and etched in a corrosive solution (5 g $FeCl_2$ + 2 ml HCl + 96 ml C_2H_5OH). The structure and the thickness of the nitriding layer were then examined using an optical microscope equipped with a micrometer. The hardness of the cross-sections of the nitrided specimens and at the surface was measured using a micro-Vickers hardness tester.

TABLE I Chemical composition of the specimen used (wt %)

C	Si	Mn	P	S	Cr	Ni	Cu
0.034	0.36	1.76	0.034	0.012	18.00	9.23	0.17

Two different X-ray diffraction techniques, 2θ–θ and GIXD, were used to identify the nitrides that had formed in the specimens. Co$K\alpha$ irradiation was used in both cases. GIXD (Model 2655Al, Rigaku-denki Co. Ltd., Tokyo) was used to identify those nitrides that had formed at the specimen surface. Using this technique, X-ray diffraction is carried out at diffraction angles of 10° to 100° and incident angles of α = 0.1° to 2.0°. After being mechanically polished close to the nitriding front, as shown later, the nitrided specimen was examined using the 2θ–θ technique at angles of from 40° to 120° to identify the nitride that had formed in the internal nitriding layer.

3. Results and discussion

Fig. 1 shows the microstructure of the nitrided Fe–18Cr-9Ni alloy. Two different nitriding layers are distinguishable: an external nitriding layer (white part) and an internal nitriding layer (grey part). The external nitriding layer is defined as the region which contains iron nitrides and nitrides of the alloying elements (CrN in this study). The internal nitriding layer is defined as the region containing nitrides of the alloying elements (Cr_2N in this study) but no iron nitrides. This figure shows that the advance of the nitriding front, F, and the interface, S^{in}, are slightly ragged in respect to the specimen surface, and that the external nitriding layer grows to about 6 to 10 μm in thickness. The external nitriding layer can be expected to have the practical property of corrosion resistance because it maintains metallic brightness after etching using a corrosive solution.

Fig. 2 shows the hardness profile on the cross-section of the nitrided alloy. Dashed lines in this figure indicate the nitriding front as determined from microstructural observations. The hardness increases to HV = 1000 to 1100 throughout the internal nitriding layer, resulting mainly from the precipitation of chromium nitride. The measured hardness in this alloy is considerably higher than in other types of steel nitrided by ammonia gas nitriding. For example, Nishigori [7] showed that ammonia gas nitriding results in a hardness of HV = 820 for nitrided Fe–4.95Cr alloy. The difference in hardness between the present alloy and Fe–4.95Cr alloy may be ascribed to differences in the

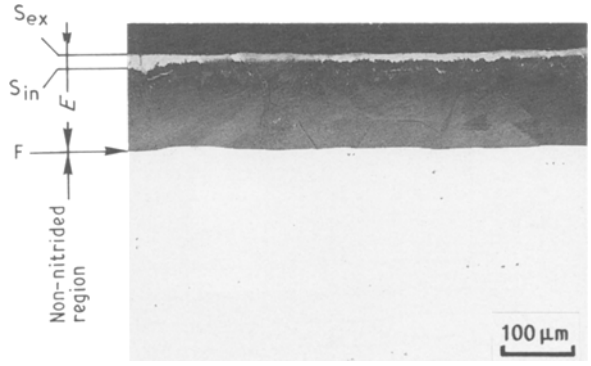

Figure 1 Microstructure of the nitriding layer formed by ammonia gas nitriding at 823 K for 68.4 ksec. S^{ex} is the specimen surface, S^{in} the interface between the external nitriding layer and the internal nitriding layer, F the nitriding front, and E the thickness of the internal nitriding layer.

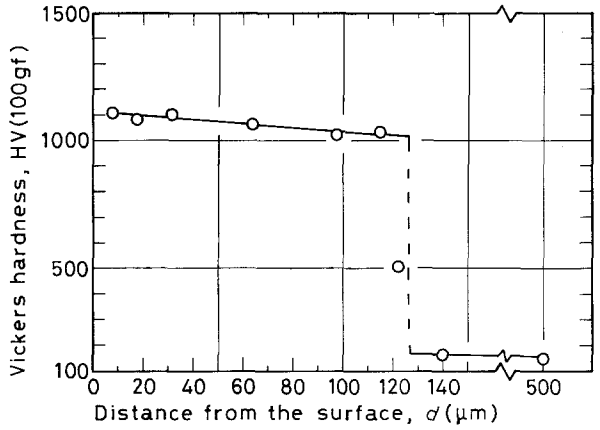

Figure 2 Hardness distribution over the cross-section of nitriding layer formed by ammonia gas nitriding at 823 K for 68.4 ksec.

volume fraction, and the size and the kind of chromium nitrides. The hardness profile in Fig. 2 can also be expected to provide high wear resistance. Accordingly, this *in situ* ammonia gas nitriding process including preheating can be expected to give both high corrosion resistance and wear resistance to the present alloy.

Fig. 3 shows the GIXD patterns, (a) at the surface of a specimen water quenched after nitriding and (b) about 5 μm beneath the specimen surface and corresponding to the region near the interface, S^{in} in Fig. 1 between the external and internal nitriding layer. α in this figure represents the incident angle of X-rays. As the incident angle increases, the X-rays penetrate deeper; that is, the results of GIXD make clear the change in structure with the depth of the external nitriding layer. Because the volume fraction of each phase is not clearly determined, it is difficult to determine the depth of X-ray penetration in specimens consisting of multiple phases.

Fig. 3a shows that the iron nitrides and the chromium nitride coexist at the surface with Fe_3O_4 even at incident angles of 0.1°. However, the volume fraction of Fe_3O_4 required from the ratio of the integral intensity of X-rays shows the maximum value at the incident angle of $\alpha = 0.2°$. Assuming that it is completely covered with Fe_3O_4, the X-ray absorption coefficient is calculated as 224.1 cm^{-1}. The thickness of Fe_3O_4 is thus calculated from the X-ray penetration as 0.36 μm (see Appendix). At an incident angle of $\alpha = 2.0°$, the X-rays penetrate to a depth of 0.78 μm if we assume that the specimen surface consists of multiple phases (mainly Fe_3O_4, γ'-Fe_4N, and CrN) with a mean absorption coefficient of 1960 cm^{-1} (see Appendix). γ'-Fe_4N seems to have a superlattice structure, because the peak of the (1 1 0) plane of γ'-Fe_4N ($d = 0.2684$ nm [8]) was detected at $2\theta = 38.9°$. This is analogous to the results of the superlattice structure at the external nitriding layer of AISI 316L alloy nitrided at 873 K on the basis of the (1 0 0) plane spot in TEM observations [3]. ε-$Fe_{2-3}N$ may also be formed at the favourable orientation of (0 0 2) at the specimen surface, if a peak of $2\theta = 48.2°$ results from the (0 0 2) diffraction of ε-$Fe_{2-3}N$ as well as (1 1 1) of γ'-Fe_4N. No austenitic or ferritic phases were detected in surface layers of less than about 1 μm.

In Fig. 3b, both austenitic ($2\theta = 50.5°$), γ, and ferritic phases ($2\theta = 52.2°$), γ_d, were identified about 5 μm from the specimen surface at incident angles of $\alpha \geqslant 1.0°$, though the austenitic phase is not observed at an incident angle of $\alpha = 0.3°$. This result indicates that there was no austenitic phase in the external nitriding layer. In the case of the alloy used in the present study, the ferritic phase, γ_d, is well known to be easily transformed from austenite by deformation on mechanical elimination of the surface layer [9]. In order to discuss the formation of γ_d, the non-nitriding specimen was analysed using X-ray diffraction after solid solution treatment. No ferritic phase peak was observed in specimens when the surface oxide layer was chemically eliminated after solid solution treating. Therefore, the γ_d in Fig. 3b, may form as a result of deformation-induced transformation of the austenitic phase due to mechanical polishing. Accordingly, the austenitic phase exists at about 5 μm beneath the specimen surface, because Fig. 3b shows the GIXD pattern of the inner region beneath about 5 μm of the specimen surface of (a). This corresponds to the interface, S^{in}, in Fig. 1.

Fig. 4 shows that three phases, γ, γ_d, and Cr_2N, were simultaneously detected in the internal nitriding layer by 2θ–θ diffraction technique. The diffraction angle, 2θ, of the austenitic phase in the internal nitriding layer shifted slightly to a higher angle with distance from the interface. This X-ray diffraction peak shift is related to the change of the lattice constant in the austenite with the dissolved nitrogen content. This

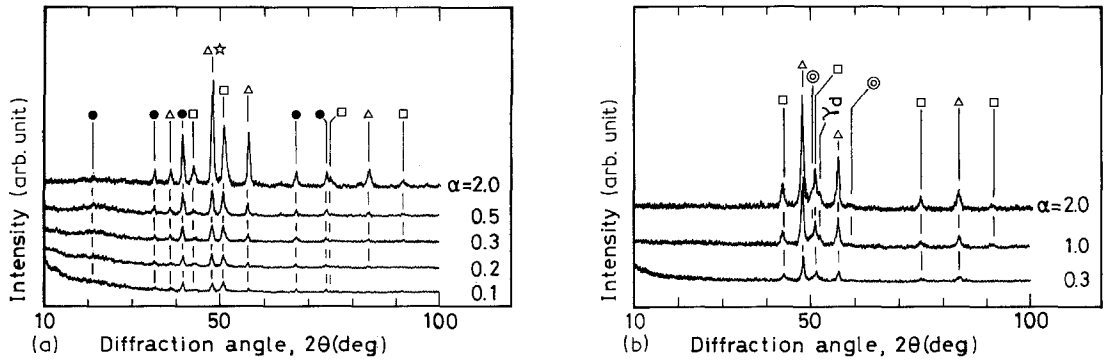

Figure 3 Grazing incidence X-ray diffraction (Co$K\alpha$) patterns for the water quenched specimen. (a) After ammonia gas nitriding at 823 K for 68.4 ksec at the specimen surface, and (b) inside the external nitriding layer within about 5 μm beneath the surface of (a). (△) γ'-Fe_4N, (□) CrN, (◎) austenite, (●) Fe_3O_4, and (☆) ε-$Fe_{2-3}N$, and γ_d ferrite transformed from austenite by induced deformation.

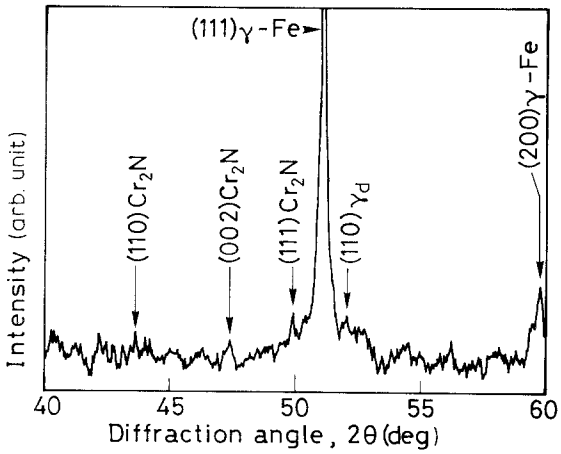

Figure 4 X-ray diffraction (Co$K\alpha$) pattern in the vicinity of the nitriding front found by the 2θ–θ technique for the specimen ammonia gas nitrided at 823 K for 68.4 ksec. γ_d represents ferrite transformed by deformation induced by austenite.

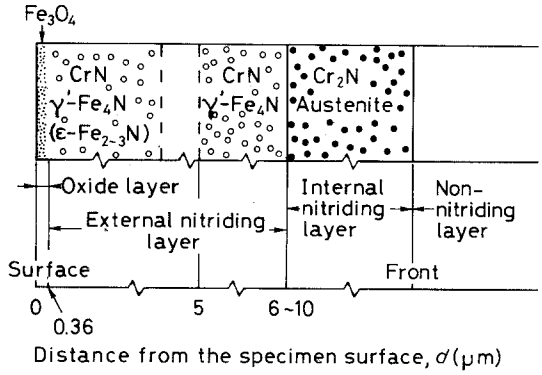

Figure 5 The schematic illustration of the nitriding layer for Fe–18Cr–9Ni alloy nitrided at 823 K for 68.4 ksec in ammonia gas.

may indicate that the dissolved nitrogen decreases with the increase in distance from the interface, S^{in} in Fig. 1. CrN, which was detected in the surface region (see Fig. 3), was not observed in the internal nitriding layer.

There have been a number of investigations into the precipitation of chromium nitrides. For example, Billon and Hendry [3] found both CrN and Cr_2N precipitates in the internal nitriding layer by gas nitriding of AISI 316L austenitic stainless steel, and the presence of Cr_2N in a ferrite matrix. Mortimer *et al.* [2] showed that with less than 20 wt % Cr, the stable phase is CrN; with more than this critical content, Cr_2N is always formed at high temperatures and CrN at lower temperatues. Nihira and Sasajima [10] described the nitrides formed by ammonia gas nitriding at 823 K for Fe–13Cr–C alloys as follows: the external nitriding layer at the surface consisted of ε–$Fe_{2-3}N$, γ'–Fe_4N, and CrN independent of carbon content, and the CrN peak was identified in the internal nitriding layer with a matrix of α–Fe and an iron carbide of Fe_3C. In the present study, however, CrN with γ'–Fe_4N precipitates in the external nitriding layer as shown in Fig. 3 and Cr_2N with γ in the internal nitriding layer as shown in Fig. 4. This indicates that the total concentration of nitrogen is higher in the external nitriding layer (CrN) than in the internal layer (Cr_2N).

Thus, the schematic construction of the nitriding layers as summarily described above can be shown in Fig. 5. The nitriding layer consists mainly of an external nitriding layer and an internal nitriding layer. The external nitriding layer is made up of a number of characteristic layers; the first is a thin Fe_3O_4 layer, the second consists of a small but favourably oriented amount of ε–$Fe_{2-3}N$ and γ'–Fe_4N with the superlattice structure, and the third layer consists of γ'–Fe_4N and CrN. This is followed by the internal nitriding layer, which consists of Cr_2N and austenite.

Although CrN is the stable phase for Fe–Cr–N alloys with less than 20 wt % Cr in the temperature range 773 to 1273 K [2], Cr_2N was observed in the internal nitriding layer of the present alloy. It is possible that the precipitation of Cr_2N in the internal nitriding layer is due to the external nitriding layer, which consists of multiple phases, preventing an adequate supply of nitrogen from being available for the conversion of Cr_2N to CrN.

4. Conclusions

To investigate the possibility of ammonia gas nitriding and to determine the nitrides formed at low temperatures below 873 K, Fe–18Cr–9Ni alloy was nitrided in ammonia gas at 823 K after hydrogen annealing at 1273 K. Microstructural observations, hardness measurements and X-ray diffraction experiments were conducted.

The main conclusions are as follows.

1. The reduction of surface oxides from the use of low-pressure hydrogen gas in the *in situ* pretreatment process makes the ammonia gas nitriding of Fe–18Cr–9Ni alloy possible at 823 K.

2. The specimen surface is completely covered with nitrides, consisting mainly of γ'–Fe_4N and CrN, which form an external nitriding layer. This layer is not etched by an acid solution of $FeCl_2$, HCl, and C_2H_5OH.

3. Ammonia gas nitriding of Fe–18Cr–9Ni alloy precipitates Cr_2N in the internal nitriding layer, throughout which the hardness is up to HV = 1000.

4. Water cooling after ammonia gas nitriding of Fe–18Cr–9Ni alloy results in the formation of iron oxide (Fe_3O_4).

Acknowledgement

The authors thank K. Kimura for his help with X-ray diffraction work.

Appendix [11]

We can calculate the X-ray penetration depth using the following equation:

$$t = -\ln(1 - y)/\mu_m(1/\sin\alpha + 1/\sin\beta) \quad \text{(A1)}$$

where t is the depth of X-ray penetration, y the percentage of the detectable decayed X-rays, μ_m the mean absorption coefficient of the X-rays, and α the grazing incident angle of the X-ray. β has the following relation between α and the diffraction angle, θ

$$\beta = 2\theta - \alpha \quad \text{(A2)}$$

In the present study, where a number of phases coexisted in the external nitriding layer, we first determined the volume fraction of each phase from the

intensity of GIXD, and then calculated μ_m using the following relation

$$\mu_m = \rho_m \sum (\mu/\rho)w \quad \text{(A3)}$$

where ρ_m is the mean density, μ the X-ray absorption of each constitutional phase, ρ the density of each constituent phase, and w the weight percentage of each constituent phase. The integral intensity per unit length of the diffracton, I, can be acquired from

$$I = (I_0 e^4/m^2c^4)\,(\lambda^3 A/32\pi r)\,(1/v^2) \times [|F|^2 p((1 + \cos^2 2\theta)/\sin^2\theta \cos\theta)\, e^{-2M}/2\mu] \quad \text{(A4)}$$

where I_0 is the intensity of the incident X-ray beam, e the electronic charge, m the mass of electron, c the velocity of light, λ the wavelength of the incident X-rays, A the cross-section of the incident X-ray beam, r the radius of the diffractometer, v the volume of the unit cell, F the structure factor, p the multiple factor, θ the Bragg angle, e^{-2M} the temperature factor, and μ the X-ray absorption coefficient. The volume fraction of each phase can be acquired using Equation A4 when multiple phases coexist. Accordingly Equations A1 to A4 give the X-ray penetration depth.

References

1. J. F. ECKEL and T. B. COX, *J. Mater.* **3** (1968) 605.
2. B. MORTIMER, P. GRIEVESON and K. H. JACK, *Scand. J. Metall.* **1** (1972) 203.
3. B. BILLON and A. HENDRY, *Surf. Engng* **1** (1985) 114.
4. T. MASUMOTO and Y. IMAI, *J. Jpn Inst. Metals* **33** (1969) 1364.
5. J. TAKADA, Y. OHIZUMI, H. MIYAMURA, H. KUWAHARA, S. KIKUCHI and I. TAMURA, *J. Mater. Sci.* **21** (1986) 2493.
6. Y. ARNAUD, M. BRUNEL, A. M. De BECDELIEVRE, M. ROMAND, P. THEVENARD and M. ROBELT, *Appl. Surf. Sci.* **26** (1986) 12.
7. S. NISHIGORI, *Denkiseikou* **10** (1934) 305.
8. Joint Committee of Powder Diffraction Standards, Card No. 6-0627.
9. M. HASEGAWA (ed.), in "Handbook of Stainless Steels" (Nikkankougyou News Papers, Tokyo, 1976) pp. 58, 85, 158, 427 (in Japanese).
10. N. NIHIRA and T. SASAJIMA, *Tetsu to Hagane* **68** (1979) S1030.
11. B. D. CULLITY, in "Elements of X-ray Diffraction" (Addison-Wesley, Massachusetts, 1974) pp. 189, 392.

Received 2 May
and accepted 29 September 1989